



## Scaling of Charge-Changing Interaction Cross Sections and Point-Proton Radii of Neutron-Rich Carbon Isotopes

T. Yamaguchi,<sup>1,\*</sup> I. Hachiuma,<sup>1</sup> A. Kitagawa,<sup>2</sup> K. Namihira,<sup>1</sup> S. Sato,<sup>2</sup> T. Suzuki,<sup>1</sup> I. Tanihata,<sup>3</sup> and M. Fukuda<sup>4</sup>

<sup>1</sup>*Department of Physics, Saitama University, Saitama 338-8570, Japan*

<sup>2</sup>*National Institute of Radiological Sciences, Chiba 263-8555, Japan*

<sup>3</sup>*Research Center for Nuclear Physics (RCNP), Osaka University, Ibaraki, Osaka 567-0047, Japan*

<sup>4</sup>*Department of Physics, Osaka University, Osaka 560-0043, Japan*

(Received 5 April 2011; published 13 July 2011)

Charge-changing cross sections  $\sigma_{cc}$  of stable and unstable nuclei ( $^9\text{--}^{11}\text{Be}$ ,  $^{14\text{--}16}\text{C}$ , and  $^{16\text{--}18}\text{O}$ ) on a carbon target were investigated at 300 MeV/nucleon. A phenomenological analysis based on the Glauber theory indicates an approximate, but universal, scaling of  $\sigma_{cc}$  over a wide range of  $A/Z$ . This allows the determination of the density distributions of protons tightly bound in the nuclei. An application to  $^{16}\text{C}$ , which is considered to be an anomalously deformed nucleus, indicates a systematic evolution of proton root-mean-square radii and has revealed for the first time a neutron skin effect in carbon isotopes. Being complementary to isotope-shift and electron-scattering experiments, the present method can open up a new approach to explore the structure of exotic nuclei.

DOI: 10.1103/PhysRevLett.107.032502

PACS numbers: 21.10.Ft, 21.10.Gv, 25.60.-t, 27.20.+n

Charge radii are basic nuclear ground-state properties. Accurate knowledge of these quantities is indispensable for exploring the evolution of shell structure in unstable nuclei. Recently, high precision measurements of charge radii of neutron-rich He [1], Li [2], and Be [3] nuclides have successfully been performed by using the laser spectroscopy technique. Neutron halo structure, manifested by the neutron density extended to extraordinarily large radial distances, was observed among these isotopes. Ever since the discovery of the nuclear halo, it has been postulated that halo neutrons are well decoupled from the core part of the nucleus. High precision experiments, however, have clearly revealed that the presence of valence neutrons enhances the charge radii of the core nuclei as compared to the corresponding nuclei without the valence neutrons. For example, the charge radius of  $^{11}\text{Li}$  is found to be larger than that of  $^9\text{Li}$ , the core nucleus of  $^{11}\text{Li}$  [2].

The isotope-shift measurements have so far provided the highest precision for the charge radii of unstable nuclei. Also, electron-scattering experiments on unstable nuclei are under way at the radioactive ion beam facilities worldwide [4,5]. However, both methods have certain limitations on their applicability mainly due to a low luminosity of rare isotopes close to the neutron drip line. Here we propose an alternative feasible methodology to derive the radii for point-proton distributions (point-proton radii) in neutron-rich nuclei and thereby easily access exotic properties near the drip line.

Based on an assumption of peripheral collisions of heavy ions at intermediate energies, a charge-changing cross section  $\sigma_{cc}$  reflects a collision probability of the valence proton(s) of the projectile with the target nucleus, thus having a sensitivity to the proton distribution [6–8].

In previous studies, we have shown the applicability of a Glauber-type analysis to obtain the proton radii of stable isotopes around  $A/Z = 2$  [9].

In this Letter, we report on precision measurements and a phenomenological analysis of  $\sigma_{cc}$  for stable and unstable nuclei, namely, for  $^9\text{--}^{11}\text{Be}$ ,  $^{14\text{--}16}\text{C}$ , and  $^{16\text{--}18}\text{O}$  nuclei reacting with a carbon target at approximately 300 MeV/nucleon. The known charge radii of Be and O isotopes were used as an input in the Glauber-type calculations in order to obtain the ratios of experimental and calculated  $\sigma_{cc}$ . The resultant  $\sigma_{cc}$  ratios were found to be nearly constant in a wide range of  $A/Z$  up to  $A/Z \approx 3$ , corresponding to a typical one-neutron halo nucleus  $^{11}\text{Be}$ . In this work we discuss in detail the results obtained for carbon isotopes.

The experiment has been performed in a similar way as the previous ones [9]. The measurements were carried out by using the fragment separator [10] at the synchrotron facility Heavy Ion Medical Accelerator in Chiba, Japan. A primary beam of  $^{18}\text{O}$  ions at an energy of 400 MeV/nucleon impinged on the beryllium production target (20–45 mm in thickness). Secondary beams were produced in the projectile fragmentation reaction. The separation of the secondary beams was realized by employing the  $B\rho\text{--}\Delta E\text{--}B\rho$  technique. To introduce the energy loss  $\Delta E$ , an aluminum wedge degrader (10–50 mm in central thickness) has been placed at the first dispersive focal plane ( $F1$ ) of the separator beam line (see Fig. 1 in Ref. [9] for the detailed beam line description).

The principle of  $\sigma_{cc}$  measurements is the transmission method. The charge-changing cross section  $\sigma_{cc}$  is determined from the equation  $\sigma_{cc} = -\frac{1}{t} \ln(\frac{\Gamma}{\Gamma_0})$ , where  $\Gamma$  and  $\Gamma_0$  represent the ratios of the number of particles with the same  $Z$  to the number of incoming projectiles for the

target-in and the target-out cases, respectively, and  $t$  denotes the number of target nuclei per unit area. The carbon target was positioned at the third focal plane ( $F3$ ). The target thickness was  $3.767 \text{ g/cm}^2$ . The thickness variation is negligible.

Upstream of the carbon target, each incident particle has been identified event by event by the  $B\rho\text{-}\Delta E\text{-TOF}$  technique to avoid contaminants. The amount of contaminants was estimated in the off-line analysis to be less than about  $10^{-5}$ . The energy-loss analysis  $\Delta E$  was performed by using two silicon detectors ( $500$  and  $450 \text{ }\mu\text{m}$  thick) located at the focal planes  $F2$  and  $F3$ , respectively. Two sets of plastic scintillation counters ( $13$  and  $0.5 \text{ mm}$  thick) placed at the  $F1$  and  $F3$  focal planes, respectively, provided the time-of-flight information. A large plastic scintillator ( $100 \times 50 \text{ mm}^2$ ,  $2 \text{ mm}$  thick) with a  $14\text{-mm}$  hole in the center, aligned with the beam line axis, ensured the nuclides of interest hitting the carbon target and avoided pileup events. Two parallel-plate avalanche counters [11] were used to center the beam on the carbon target. A typical particle identification is shown in Fig. 1(a) on the example of  $^{16}\text{C}$  production.

Downstream of the target, a stack of six silicon detectors ( $450 \text{ }\mu\text{m}$  thick each) was used to measure  $\Delta E$  of the outgoing particles. The solid angle coverage of the silicon telescope was  $\pm 10^\circ$ , which is large enough to measure all projectiles penetrating through the carbon target. The sum of  $\Delta E$  from the silicon detectors allows unambiguous identification of charges of the outgoing particles. A  $\Delta E$  resolution of  $2.2\%$  ( $1\sigma$ ) has been obtained for the  $^{18}\text{O}$  primary beam. A  $5\text{-mm}$  CsI(Tl) scintillation counter was also employed for the  $\Delta E$  analysis. A clear  $Z$  separation

for  $^{16}\text{C}$  was observed in a two-dimensional correlation plot of  $\Delta E$  from the CsI(Tl) scintillator versus the  $\Delta E$  sum of the silicon detectors. It is shown in Fig. 1(b). Channeling and reaction events in the silicon detectors, which generally produce smaller and larger pulse heights, respectively, than those of the projectiles, were properly analyzed as noninteracting events. The event selection gates applied to the  $\Delta E$  spectra might introduce a systematic uncertainty in the  $\sigma_{\text{cc}}$ . This was confirmed by changing the gate width for the  $\Delta E$  spectra. The deduced variations were added quadratically to the total errors. The results obtained from the CsI(Tl) counter are consistent with those from the stack detector. Thus obtained results of  $\sigma_{\text{cc}}$  are tabulated in Table I and are graphically shown in Figs. 1(c)–1(e).

In order to investigate the relation between  $\sigma_{\text{cc}}$  and the point-proton distributions, we performed zero-range optical-limit Glauber-type calculations [12] with the phenomenological correction factor [9]. A charge-changing cross section  $\sigma_{\text{cc}}$  is described by the following equations:

$$\sigma_{\text{cc}} = 2\pi \int b[1 - T^p(b)]\mathcal{E}(E)db,$$

$$T^p(b) = \exp\left[-\left(\sigma_{pp} \int \rho_p^{\text{targ}} \rho_p^{\text{proj}} + \sigma_{np} \int \rho_n^{\text{targ}} \rho_p^{\text{proj}}\right)\right], \quad (1)$$

where  $b$  denotes the impact parameter and  $\sigma_{pp}$  ( $\sigma_{np}$ ) the proton(neutron)-proton cross sections.  $T^p(b)$  is a part of the transmission function, where  $\rho_p^{\text{targ}}$  ( $\rho_n^{\text{targ}}$ ) is the  $z$ -integrated density distribution of protons (neutrons) in the target and  $\rho_p^{\text{proj}}$  is that of protons in the projectile. The phenomenological correction factor  $\mathcal{E}(E)$  was determined to be  $1.12$  at  $300 \text{ MeV/nucleon}$  from precise experimental  $\sigma_{\text{cc}}$  values [9]. A harmonic oscillator (HO) density distribution [13] was applied to the carbon target. The width parameter of the HO density was determined to be  $a_{\text{HO}}(^{12}\text{C}) = 1.645 \text{ fm}$ , which reproduces the experimental interaction cross section of  $^{12}\text{C}$  on carbon at  $950 \text{ MeV/nucleon}$  [13].

TABLE I. Results on  $\sigma_{\text{cc}}^{\text{expt}}$  for  $^9\text{--}^{11}\text{Be}$ ,  $^{14}\text{--}^{16}\text{C}$ , and  $^{16}\text{--}^{18}\text{O}$  isotopes on a carbon target. Listed in the second column are the energies in the middle of the target. The  $\sigma_{\text{cc}}^{\text{calc}}$  obtained from known charge radii are given in the last column.

Nuclide	$E$ (MeV/nucleon)	$\sigma_{\text{cc}}^{\text{expt}}$ (mb)	$\sigma_{\text{cc}}^{\text{calc}}$ (mb)
$^9\text{Be}$	276	$730 \pm 8$	621
$^{10}\text{Be}$	280	$647 \pm 8$	594
$^{11}\text{Be}$	277	$659 \pm 11$	614
$^{14}\text{C}$	287	$731 \pm 5$	716
$^{15}\text{C}$	285	$743 \pm 6$	...
$^{16}\text{C}$	284	$726 \pm 6$	...
$^{16}\text{O}$	288	$852 \pm 17$	832
$^{17}\text{O}$	294	$896 \pm 9$	829
$^{18}\text{O}$	299	$891 \pm 10$	849

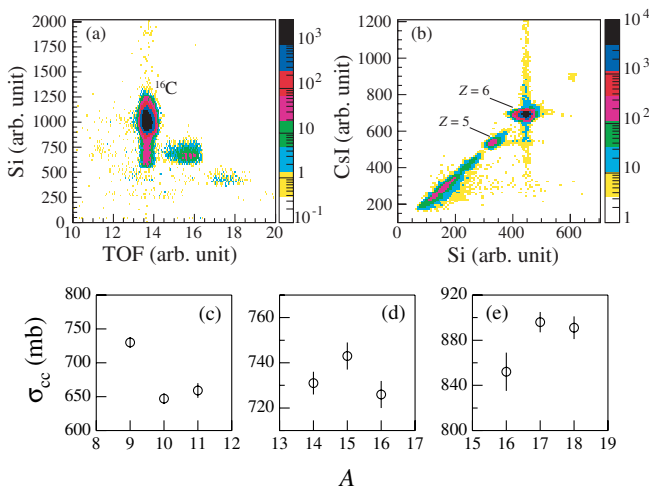


FIG. 1 (color online). Particle identifications of  $^{16}\text{C}$  (a) before and (b) after the carbon target. (a) Two-dimensional plot of  $\Delta E$  from the silicon detector at  $F2$  versus time-of-flight between  $F1$  and  $F3$ . (b) Correlation plot of the  $\Delta E$  counters after the carbon target, CsI(Tl) scintillator versus the  $\Delta E$  sum of silicon detectors. Results of  $\sigma_{\text{cc}}$  as a function of mass number for (c) Be, (d) C, and (e) O isotopes.

The HO density was also applied to the proton density functions of the projectiles with known charge radii ( ${}^9\text{--}{}^{11}\text{Be}$  [3],  ${}^{14}\text{C}$  [14], and  ${}^{16\text{--}18}\text{O}$  [14]). The width parameters  $a_{\text{HO}}^p$  were determined to reproduce the root-mean-square (rms) radii  $\tilde{r}_p$  of the point-proton distributions. The  $\tilde{r}_p$  was calculated to be  $\tilde{r}_p^2 = \tilde{r}_{\text{ch}}^2 - \langle R_p^2 \rangle - \frac{N}{Z} \times \langle R_n^2 \rangle - \frac{3\hbar^2}{4m_p^2 c^2}$ , where  $\tilde{r}_{\text{ch}}$  is the rms charge radius,  $\langle R_p^2 \rangle$  and  $\langle R_n^2 \rangle$  are the proton and neutron mean-square charge radii, respectively [ $\langle R_p^2 \rangle^{1/2} = 0.895(18)$  fm [15] and  $\langle R_n^2 \rangle = -0.1149(24)$  fm<sup>2</sup> [16]], and the last term is the Darwin-Foldy correction [17].

Applying Eq. (1), the charge-changing cross sections  $\sigma_{\text{cc}}^{\text{calc}}$  have been calculated for  ${}^9\text{--}{}^{11}\text{Be}$ ,  ${}^{14}\text{C}$ , and  ${}^{16\text{--}18}\text{O}$  and are presented in Table I. The ratios of experimental  $\sigma_{\text{cc}}^{\text{expt}}$  and calculated  $\sigma_{\text{cc}}^{\text{calc}}$  values are indicated with filled symbols (circles:  ${}^9\text{--}{}^{11}\text{Be}$ ; square:  ${}^{14}\text{C}$ ; triangles:  ${}^{16\text{--}18}\text{O}$  isotopes) in Fig. 2. As a result, we find that the ratios are approximately constant over a wide range of  $Z/N$ ;  $\mathcal{F} = \sigma_{\text{cc}}^{\text{expt}}/\sigma_{\text{cc}}^{\text{calc}} = 1.05 \pm 0.03$ , within a standard deviation of  $\pm 3\%$  shown by the shaded area in Fig. 2. The constancy of the  $\sigma_{\text{cc}}$  ratio suggests that the direct proton removal channel dominates the charge-changing process at the present energy. We emphasize that the typical one-neutron halo nucleus  ${}^{11}\text{Be}$  follows the present scaling. The ratio for  ${}^9\text{Be}$  is equal to 1.17 ( $Z/N = 0.8$ ) and thus shows a large deviation. This can be explained by the one-neutron removal channel in  ${}^9\text{Be}$  which contributes to the charge-changing cross section yielding unbound  ${}^8\text{Be}$  nuclei breaking immediately up into two  $\alpha$  particles. The high-energy data [6] for nuclides with known charge radii ( ${}^{10,11}\text{B}$ ,  ${}^{12,13}\text{C}$ ,  ${}^{14,15}\text{N}$ , and  ${}^{19}\text{F}$ ) were scaled to the present energy. They were used to calculate the  $\sigma_{\text{cc}}$  ratios in the same way

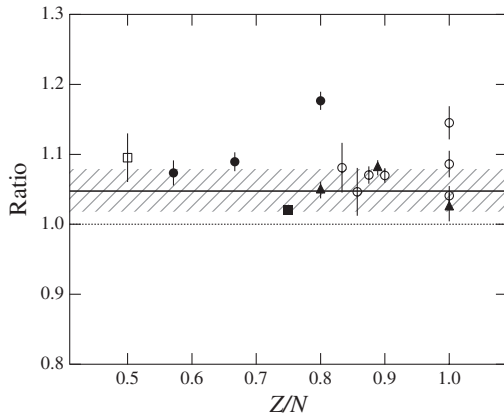


FIG. 2. Results on the ratios of experimental  $\sigma_{\text{cc}}^{\text{expt}}$  and calculated  $\sigma_{\text{cc}}^{\text{calc}}$  as a function of  $Z/N$  for the nuclei with the known charge radii  ${}^9\text{--}{}^{11}\text{Be}$  (filled circles),  ${}^{14}\text{C}$  (filled square), and  ${}^{16\text{--}18}\text{O}$  (filled triangles) isotopes. The solid line and the shaded band show the result of the least square fitting of the experimental data with the corresponding standard deviations, respectively. The open square and circles show the ratios for  ${}^9\text{Li}$  and the high-energy data scaled to the present energy [6].

as described above and are plotted in Fig. 2 as open circles. A largely deviating ratio at around 1.15 at  $Z/N = 1$  comes from  ${}^{10}\text{B}$ . It is caused by the same reason as in the case of  ${}^9\text{Be}$ . Thus, the overall results agree well within their uncertainties with the present scaling. This indicates an approximate but universal scaling of  $\sigma_{\text{cc}}$ . Thus, results might be due to the fact that the beam energy lies in the minimum of the nucleon-nucleon cross sections; that is, the reaction complexity relevant for the nucleus-nucleus collisions is minimal. The present method allows the determination of the density distributions of protons “embedded” into neutron-rich nuclei.

The application of the method to the carbon isotopes yields valuable information on their proton radii which are difficult to determine by the laser spectroscopy technique. The first measurement of  $B(E2)$  in  ${}^{16}\text{C}$  suggested an anomalous deformation [18]. This stimulated intensive studies of the  $B(E2)$  values [19,20] as well as inelastic scattering experiments with  ${}^{16}\text{C}$  [21]. Our new results on  $\sigma_{\text{cc}}$  of  ${}^{15,16}\text{C}$  can provide an additional constraint on the shell structure evolution in carbon isotopes.

By applying the present  $\sigma_{\text{cc}}$  scaling, the point-proton radii of  ${}^{15,16}\text{C}$  can be determined from the measured charge-changing cross sections. Assuming the HO density for the proton density distributions of these nuclei, the width parameters were determined which reproduce the measured  $\sigma_{\text{cc}}^{\text{expt}}/\mathcal{F}$ . The rms point-proton radii of  ${}^{15}\text{C}$  and  ${}^{16}\text{C}$  have been determined to be  $\tilde{r}_p = 2.33 \pm 0.11$  fm and  $\tilde{r}_p = 2.25 \pm 0.11$  fm, respectively. The main contribution to the experimental errors comes from the variation of the scaling factor. Although the uncertainties for the radii are still rather large, the new results are consistent with those for the stable carbon isotopes and support the systematic evolution of the proton radii in this region (see Table II). We note that the proton radius of  ${}^{16}\text{C}$  is on the downward trend as compared to that of  ${}^{14}\text{C}$ . Adding neutrons to a stable nucleus generally causes a decrease of the charge radius, which had been qualitatively explained by Bohr and Mottelson [23].

The nuclear matter radii of  ${}^{15,16}\text{C}$  have been precisely determined from the interaction cross sections measurements at high energies (see Table II) [22]. Therefore, our new proton radii enabled us to derive the neutron radii of these nuclei. This was done by employing the relation  $\tilde{r}_m^2 = \frac{Z}{A} \tilde{r}_p^2 + \frac{N}{A} \tilde{r}_n^2$ , where  $\tilde{r}_m$ ,  $\tilde{r}_p$ , and  $\tilde{r}_n$  are the rms matter,

TABLE II. Root-mean-square point-proton ( $\tilde{r}_p$ ) and matter ( $\tilde{r}_m$ ) radii of carbon isotopes.

Nuclide	$\tilde{r}_p$ (fm)	$\tilde{r}_m$ (fm)
${}^{12}\text{C}$	$2.320 \pm 0.007$ [14]	$2.31 \pm 0.02$ [22]
${}^{13}\text{C}$	$2.315 \pm 0.008$ [14]	$2.28 \pm 0.04$ [22]
${}^{14}\text{C}$	$2.364 \pm 0.011$ [14]	$2.30 \pm 0.07$ [22]
${}^{15}\text{C}$	$2.33 \pm 0.11$	$2.48 \pm 0.03$ [22]
${}^{16}\text{C}$	$2.25 \pm 0.11$	$2.70 \pm 0.03$ [22]

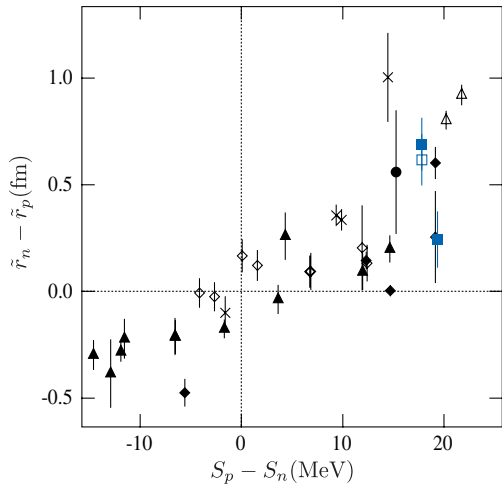


FIG. 3 (color online). Difference of the neutron and proton radii as a function of the difference of the proton and neutron separation energies  $S_p - S_n$ .  ${}^6,8\text{He}$  isotopes [1] are indicated with open triangles,  ${}^{6,8,9,11}\text{Li}$  [2] with crosses,  ${}^{7,9-11}\text{Be}$  with filled diamonds,  ${}^{20}\text{N}$  [27] with the filled circle, neutron-rich Na isotopes [24] with filled triangles, and proton-rich Ar isotopes [25] with open diamonds. Our new results on  ${}^{15,16}\text{C}$  isotopes are shown with filled (blue) squares. The open square corresponds to the  ${}^{16}\text{C}$  result with the deformation effect included.

proton, and neutron radii, respectively. The neutron skin thicknesses  $\tilde{r}_n - \tilde{r}_p$  have been calculated and are plotted as a function of the difference of the proton and neutron separation energies  $S_p - S_n$  in Fig. 3 (filled squares). The skin thicknesses for He [1], Li [2], Be [3], Na [24], and Ar isotopes [25] are plotted for comparison. The present results on the carbon isotopes are consistent with the general trend of the skin thicknesses which correlate linearly with  $S_p - S_n$ .

Different deformations of proton and neutron shapes in the  ${}^{16}\text{C}$  nucleus have been proposed [26]. The quadrupole deformation effect enhances the radius as  $\tilde{r}^{\text{def}} = \tilde{r}^{\text{sph}} \sqrt{1 + (5/4\pi)\beta^2}$ , where  $\tilde{r}^{\text{def}}$  and  $\tilde{r}^{\text{sph}}$  are the deformed and spherical components of the radius, respectively, and  $\beta$  is the deformation parameter. In the calculations above, the deformed components  $\tilde{r}_p^{\text{def}}$  and  $\tilde{r}_n^{\text{def}}$  of  ${}^{16}\text{C}$  have been used to evaluate the skin thickness  $\tilde{r}_n^{\text{def}} - \tilde{r}_p^{\text{def}}$ . Supposing that the deformation of  ${}^{16}\text{C}$  follows the systematic behavior of even-even nuclei in this region, that is,  $\beta \sim 0.4$  for both proton and neutron, our result for the skin thickness  $\tilde{r}_n^{\text{sph}} - \tilde{r}_p^{\text{sph}}$  is reduced by merely 3%. However, a systematic analysis of the inelastic scattering of  ${}^{16}\text{C}$  on proton and lead indicates a different deformation between proton and neutron distributions, namely,  $\beta_p = 0.3$  and  $\beta_n = 0.45$  [21]. In this case the skin thickness of  ${}^{16}\text{C}$  is reduced by 10%. This value is shown with the open square in Fig. 3. Both results clearly reveal a thick neutron skin for  ${}^{16}\text{C}$  comparable to the ones in  ${}^6\text{He}$  and  ${}^{11}\text{Be}$  halo nuclei.

In summary, we have performed the precision measurements of the charge-changing cross sections  $\sigma_{\text{cc}}$  of  ${}^9-11\text{Be}$ ,  ${}^{14-16}\text{C}$ , and  ${}^{16-18}\text{O}$  nuclides on carbon at energies around 300 MeV/nucleon. Based on the Glauber-type analysis with the phenomenological correction, we have discovered an approximate, but universal, scaling of  $\sigma_{\text{cc}}$  values over a wide range of  $A/Z$ . Our new method has successfully been applied to the carbon isotopes, revealing a systematic evolution of proton radii and the neutron skin effect. The present study may open up a new approach for future investigations of ground-state properties of exotic nuclei.

The authors are grateful to the AEC staff for the technical support and excellent accelerator operations. This work was supported by the Research Project with Heavy Ions at NIRS-HIMAC (Program No. P246). We thank Yu. A. Litvinov for commenting on this manuscript.

\*yamaguti@phy.saitama-u.ac.jp

- [1] P. Mueller *et al.*, *Phys. Rev. Lett.* **99**, 252501 (2007).
- [2] R. Sánchez *et al.*, *Phys. Rev. Lett.* **96**, 033002 (2006).
- [3] W. Nörtershäuser *et al.*, *Phys. Rev. Lett.* **102**, 062503 (2009).
- [4] T. Suda *et al.*, *Phys. Rev. Lett.* **102**, 102501 (2009).
- [5] [http://www.gsi.de/fair/experiments/elise/index\\_e.html](http://www.gsi.de/fair/experiments/elise/index_e.html).
- [6] L. V. Chulkov *et al.*, *Nucl. Phys.* **A674**, 330 (2000).
- [7] J. Meng, S.-G. Zhou, and I. Tanihata, *Phys. Lett. B* **532**, 209 (2002).
- [8] A. Bhagwat and Y. K. Gambhir, *Phys. Rev. C* **69**, 014315 (2004).
- [9] T. Yamaguchi *et al.*, *Phys. Rev. C* **82**, 014609 (2010).
- [10] M. Kanazawa *et al.*, *Nucl. Phys.* **A746**, 393 (2004).
- [11] H. Kumagai *et al.*, *Nucl. Instrum. Methods Phys. Res., Sect. A* **470**, 562 (2001), and references therein.
- [12] R. J. Glauber, in *Lectures in Theoretical Physics*, edited by W. E. Brittin *et al.* (Interscience, New York, 1959), Vol. 1, p. 315.
- [13] A. Ozawa, T. Suzuki, and I. Tanihata, *Nucl. Phys.* **A693**, 32 (2001).
- [14] I. Angeli, *At. Data Nucl. Data Tables* **87**, 185 (2004).
- [15] I. Sick, *Phys. Lett. B* **576**, 62 (2003).
- [16] S. Kopecky *et al.*, *Phys. Rev. C* **56**, 2229 (1997).
- [17] J. L. Friar, J. Martorell, and D. W. L. Sprung, *Phys. Rev. A* **56**, 4579 (1997).
- [18] N. Imai *et al.*, *Phys. Rev. Lett.* **92**, 062501 (2004).
- [19] M. Wiedeking *et al.*, *Phys. Rev. Lett.* **100**, 152501 (2008).
- [20] H. J. Ong *et al.*, *Phys. Rev. C* **78**, 014308 (2008).
- [21] Z. Elekes *et al.*, *Phys. Rev. C* **78**, 027301 (2008), and references therein.
- [22] A. Ozawa *et al.*, *Nucl. Phys.* **A691**, 599 (2001).
- [23] A. Bohr and B. R. Mottelson, *Nuclear Structure* (World Scientific, Singapore, 1998), Vol. 1, Chap. 2-1.
- [24] T. Suzuki *et al.*, *Phys. Rev. Lett.* **75**, 3241 (1995).
- [25] A. Ozawa *et al.*, *Nucl. Phys.* **A709**, 60 (2002); *Nucl. Phys.* **A727**, 465 (2003).
- [26] Y. Kanada-En'yo, *Phys. Rev. C* **71**, 014310 (2005).
- [27] O. V. Bochkarev *et al.*, *Eur. Phys. J. A* **1**, 15 (1998).